

# Phase-space analysis and experimental results for secondary focusing at X-ray beamlines

Rong Huang,<sup>a\*</sup> Mati Meron,<sup>b</sup> Naresh Kujala<sup>c</sup> and Raul A. Barrea<sup>c</sup>

Received 17 January 2010

Accepted 22 June 2010

<sup>a</sup>IMCA-CAT, Hauptman-Woodward Institute, USA, <sup>b</sup>CARS, University of Chicago, USA, and <sup>c</sup>Bio-CAT, Illinois Institute of Technology, USA. E-mail: rhuang@anl.gov

Micro-focusing optical devices at synchrotron beamlines usually have a limited acceptance, but more flux can be intercepted if such optics are used to focus secondary sources created by the primary optics. Flux throughput can be maximized by placing the secondary focusing optics close to or exactly at the secondary source position. However, standard methods of beamline optics analysis, such as the lens equation or matching the mirror surface to an ellipse, work poorly when the source-to-optics distance is very short. In this paper the general characteristics of the focusing of beams with Gaussian profiles by a ‘thin lens’ are analysed under the paraxial approximation in phase space, concluding that the focusing of a beam with a short source-to-optics distance is distinct from imaging the source; slope errors are successfully included in all the formulas so that they can be used to calculate beamline focusing with good accuracy. A method is also introduced to use the thin-lens result to analyse the micro-focusing produced by an elliptically bent trapezoid-shaped Kirkpatrick–Baez mirror. The results of this analysis are in good agreement with ray-tracing simulations and are confirmed by the experimental results of the secondary focusing at the 18-ID Bio-CAT beamline (at the APS). The result of secondary focusing carried out at 18-ID using a single-bounce capillary can also be explained using this phase-space analysis. A discussion of the secondary focusing results is presented at the end of this paper.

© 2010 International Union of Crystallography  
Printed in Singapore – all rights reserved**Keywords:** optics; focusing; X-ray; KB mirrors; capillary; imaging.

## 1. Introduction

X-ray optical devices capable of focusing a synchrotron beam to a few micrometers or smaller focal spot sizes normally intercept only a small portion of the total flux available at a beamline. The flux acceptance can be improved by using such a device to focus a secondary source provided by a primary focusing optics. Secondary focusing has been reported using capillaries (Huang & Bilderback, 2003; Snigirev *et al.*, 2007; Barrea *et al.*, 2009), Kirkpatrick–Baez (KB) mirrors (Mosselmanns *et al.*, 2009) and possibly using other optics as well. The flux delivered to the sample is maximized by positioning the secondary focusing element at the secondary source location, as is the case with the capillary secondary focusing at the Bio-CAT undulator beamline 18-ID at the Advanced Photon Source (APS), Argonne National Laboratory. Although both ray-tracing and experiment confirm that such a configuration can produce good secondary focusing and deliver very high fluxes (Barrea *et al.*, 2009), it cannot be explained by the lens equation,  $1/F = 1/z_0 + 1/z_2$ , which would predict  $z_2 \simeq 0$  but no focusing when  $z_0 \simeq 0$  ( $F$ ,  $z_0$ ,  $z_2$  are, respectively, the focal

length, source distance and image distance in this paper). That is because the focusing of an extended source is not the same as imaging the source, and quite different results are predicted when such a source is close to the optics. Such difference between focusing and imaging can be best studied in phase space, using matrix methods.

X-ray beams have been analysed using matrix methods in position-angle phase space (Hastings, 1977; Matsushita & Kaminaga, 1980a) and in position-angle-wavelength space (Matsushita & Kaminaga, 1980b; Pedersen & Riekkel, 1991; Smilgies, 2008; Ferrero *et al.*, 2008), and even for beams with an arbitrary degree of coherence (Meron *et al.*, 1999). Applying beam optics to calculate the focusing at a beamline appears to be a straightforward task, according to those previous studies. However, some details of the focusing analysis that are relevant to the understanding of focusing with arbitrary source distances are widely neglected in the beamline focusing calculations performed so far. In this paper a beam with Gaussian profile focused by a ‘thin lens’ is analysed in phase space under the paraxial approximation, with detailed discussions. The formulas derived from this thin-

lens study are then used for secondary focusing calculations. Slope errors are included in all the formulas so that they can be used to analyse the focusing performance of real beamlines, with good accuracy.

Elliptically bent trapezoid-shaped mirrors using the so-called two-parameter benders are commonly used for micro-focusing at third-generation X-ray sources (Yang *et al.*, 1995; Eng *et al.*, 1998), and can also be used as secondary focusing optics in beamlines, with focusing quality judged by a comparison between the bent-mirror profile and an ellipse determined by the source and focus locations. The difference between the mirror profile and the ideal ellipse can be very small, therefore good focusing can be achieved with these kinds of optics (Eng *et al.*, 1998). At the Bio-CAT 18-ID beamline, a 5  $\mu\text{m}$  spot with flux of  $1.3 \times 10^{12}$  photons  $\text{s}^{-1}$  is achieved using a set of trapezoid-shaped KB mirrors by directly imaging the undulator source, but with a limited acceptance owing to the small size of the mirrors. For some applications it is desirable to deliver higher flux beams and a moderate sacrifice of minimal spot size may be tolerated. A simple way to increase the flux to sample at 18-ID would be to pre-focus the incident beam slightly using the beamline main optics in order to increase the flux within the acceptance aperture of the KB mirrors. Previous calculation (Eng *et al.*, 1998) showed that, for given source and image distances, when the beam incident angle changes (so the mirror focal length and, therefore, degree of bending changes) the optimal taper factor of the mirror shape remains unchanged and that is how the taper factor of a trapezoidal mirror is determined. It was not clear, though, how good the focusing quality could be in the secondary focusing case, when the source distance changes while the trapezoidal mirror taper factor is already optimized for a direct source at the undulator location. The purpose of the present study is to analyse whether or not trapezoidal mirrors are suitable for use with a large variation of source distance and to evaluate the trade-offs between secondary focusing spot size and flux acceptance when pre-focusing. We also want such an analysis to remain valid even when the secondary source is at the KB mirror position for maximized flux acceptance. A method using the thin-lens results given in this paper to analyse the focusing by an asymmetrically bent mirror is also introduced.

In §2, phase-space analysis (under the paraxial approximation) of a beam with Gaussian profile, being focused by a thin lens with slope errors, is presented, followed by discussions. In §3, the results from §2 are used in two iterations to evaluate trapezoidal mirror secondary focusing under different pre-focusing conditions, and are also used to explain the results of a previously reported (Barrea *et al.*, 2009) single-bounce capillary secondary focusing at 18-ID. The reason why we can use the thin-lens results to calculate the focusing by a KB mirror whose curvature varies along its surface is also explained in §3. Ray-tracing simulations are used to verify the analytical calculations. In §4, experimental results using KB mirrors for X-ray secondary focusing at 18-ID are described and compared with the calculated data. The main conclusions, and associated discussion, are presented in §5.

## 2. Extended source focusing described in phase space

### 2.1. X-ray beam focusing by a thin lens with slope errors

In this paper we use the terms ‘source distance’ and ‘focus distance’ instead of the ‘object distance’ and ‘image distance’ used in Gaussian optics, because focusing is different from imaging (more details are given in this section). The focus of a beam is defined here as the beam waist (having minimal size along its path) at the image side, where the beam intensity spatial and angular profiles in phase space are not coupled [*i.e.*  $B_3 = 0$  with the profile given by equation (4)].

In each transverse direction the X-ray intensity distribution emitted by a synchrotron source can be presented in phase space as a product of two Gaussians, one for the intensity variation as a function of X-ray position and one as a function of X-ray travelling angle relative to the beam axis. Away from the source location the X-ray positional and angular profiles are, in general, coupled. So we start our analysis with a beam in the general condition, having a transverse phase-space distribution of

$$I_0(x_0, \theta_0) = k_0 \exp(-A_0x_0^2 - 2B_0x_0\theta_0 - C_0\theta_0^2), \quad (1)$$

where  $(x_0, \theta_0)$  are the conjugated coordinates as shown in Fig. 1, and  $A_0, B_0, C_0$  are related to the beam spatial and angular r.m.s. sizes by  $\sigma_{x_0}^2 = C_0/2Q_0, \sigma_{\theta_0}^2 = A_0/2Q_0, Q_0 = A_0C_0 - B_0^2$  and  $k_0 = (Q_0)^{1/2}/\pi$  when the distribution is normalized. Within the paraxial approximation, as an X-ray propagates through a thin lens having a focal length of  $F$  at distance of  $z_0$ , its position in phase space at the location of the optics will be related to its position at the source by (Gerrard & Burch, 1975)

$$\begin{bmatrix} x_2 \\ \theta_2 \end{bmatrix} = \begin{bmatrix} 1 & 0 \\ -1/F & 1 \end{bmatrix} \begin{bmatrix} x_1 \\ \theta_1 \end{bmatrix} = \begin{bmatrix} 1 & 0 \\ -1/F & 1 \end{bmatrix} \begin{bmatrix} 1 & z_0 \\ 0 & 1 \end{bmatrix} \begin{bmatrix} x_0 \\ \theta_0 \end{bmatrix}, \quad (2)$$

where the subscripts 1 and 2 represent the phase-space coordinates at the optics location right before and after, respectively, the X-ray passes the thin lens, as described in Fig. 1. The coordinate transformation  $I_0(x_0, \theta_0) = I_2[x_0(x_2, \theta_2), \alpha_0(x_2, \theta_2)]$  (Pedersen & Riekel, 1991; Huang & Bilderback, 2001; Smilgies, 2008; Ferrero *et al.*, 2008) can be used to calculate the X-ray distribution at the location of the optics, but having just passed through it, in the form of

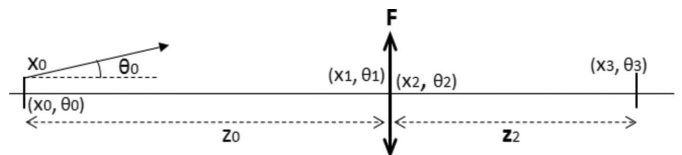


**Figure 1**

Diagram of an extended beam focused by a thin lens with focal length  $F$ . The conjugated coordinates used in phase-space analysis are shown in the figure, with  $(x_0, \theta_0)$  representing either a synchrotron source or a secondary source, and  $(x_3, \theta_3)$  the coordinates of a ray at any distance  $z_2$  downstream of the optics.  $(x_1, \theta_1)$  and  $(x_2, \theta_2)$  are the coordinates of a ray at the location of the optical element right before and after, respectively, passing through it.

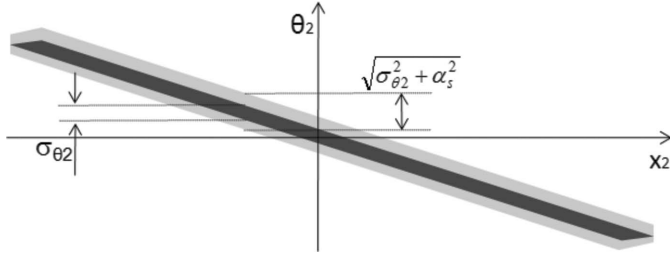


**Figure 2**  
Schematic illustration of the change of beam angular size in phase space by the slope errors of an optics from  $\sigma_{\theta 2}$  to  $(\sigma_{\theta 2}^2 + \alpha_s^2)^{1/2}$ , where  $\sigma_{\theta 2}$  is the divergence only of the rays at a given surface location of the optics, not the divergence of the whole beam.

$$I_2(x_2, \theta_2) = k_2 \exp\left[-x_2^2/2\sigma_{x2}^2 - (\theta_2 - t x_2)^2/2\sigma_{\theta 2}^2\right], \quad (3)$$

where  $t \neq 0$  because of the coupling of the distribution in phase space (while  $\sigma_{x2}$  is the r.m.s. size of the whole beam,  $\sigma_{\theta 2}$  is only the divergence of the rays at one location of the optical surface, as shown in Fig. 2). Owing to the slope errors of the optical element, the X-ray angular divergence at each location will broaden from  $\sigma_{\theta 2}$  to  $(\sigma_{\theta 2}^2 + \alpha_s^2)^{1/2}$ , where  $\alpha_s$  is the angular broadening by slope errors, given by twice the r.m.s. slope errors if the optics is a mirror.  $k_2$  in (3) needs to be modified accordingly to keep  $I_2$  normalized after substituting  $\sigma_{\theta 2}$  in (3) with  $(\sigma_{\theta 2}^2 + \alpha_s^2)^{1/2}$ . With another coordinate transformation, the X-ray intensity distribution at any distance  $z_2$  downstream of the optics can be written as

$$I_3(x_3, \theta_3) = k_3 \exp(-A_3 x_3^2 - 2B_3 x_3 \theta_3 - C_3 \theta_3^2), \quad (4)$$

where

$$k_3 = T k_0 / M^{1/2}, \quad (5a)$$

$$A_3 = \psi^2 / \Delta M + Q_0 / \Delta, \quad (5b)$$

$$B_3 = -z_2 (\psi^2 + M Q_0) / \Delta M + \psi / M, \quad (5c)$$

$$C_3 = (\Delta - z_2 \psi)^2 / \Delta M + z_2^2 Q_0 / \Delta, \quad (5d)$$

where  $T$  is either the transmission of a lens or the reflectivity of a mirror, and the other constants are

$$\Delta = A_0 z_0^2 - 2B_0 z_0 + C_0, \quad (6a)$$

$$\psi = \Delta / F - A_0 z_0 + B_0, \quad (6b)$$

$$M = 1 + 2\Delta \alpha_s^2. \quad (6c)$$

The X-ray r.m.s. size at  $z_2$  will be

$$\sigma_{x3} = (C_3 / 2Q_3)^{1/2}, \quad (7)$$

where  $Q_3 = A_3 C_3 - B_3^2$ . When  $z_2$  is right at the beam focus,  $\partial \sigma_{x3} / \partial z_2 = 0$ , it can be derived from (7) that

$$F = \left[ \Delta + 2\varphi z_2 - (\Delta^2 - 4z_2^2 Q_0 M)^{1/2} \right] / 2(\varphi + z_2 A_+), \quad (8a)$$

$$\sigma_{x3} = [M\Delta / 2(MQ_0 + \psi^2)]^{1/2}, \quad (8b)$$

$$\sigma_{\theta 3} = \{M\Delta / 2[(\Delta - z_2 \psi)^2 + MQ_0 z_2^2]\}^{1/2}, \quad (8c)$$

$$z_2 = \Delta \psi / (MQ_0 + \psi^2), \quad (8d)$$

where  $\varphi = A_0 z_0 - B_0$  and  $A_+ = A_0 + 2\alpha_s^2 Q_0$ . While equations (4), (5) and (6) can be used to calculate the phase-space

distribution of the beam at any location after an optics, equation (8) can be used to calculate the focal length  $F$  needed for focusing, the beam focal spot size and its focus distance.

If there is an aperture at location  $z_2$  with opening  $s$ , the fraction of the flux,  $p$ , that passes through the aperture can be calculated by integrating (4) over the full angular dimension and the space of slit opening,

$$p = \text{erf}[s(Q_3/C_3)^{1/2}/2]. \quad (9)$$

It can be verified using (5) and (8) that, at the beam focus (where  $\partial \sigma_{x3} / \partial z_2 = 0$ ),  $B_3 = 0$ , *i.e.* the beam intensity spatial and angular profiles are not coupled, even after an optical element with slope errors.

## 2.2. Application to typical beamline configurations

The above results can be used to explain some typical beamline focusing configurations. Assuming a beam is focused by a focusing element with no slope errors ( $\alpha_s = 0$ ), letting  $B_0 = 0$ ,  $B_3 = 0$ , *i.e.* only using beam parameters at the source and focus locations, and using  $A_0 = 1/2\sigma_{x0}^2$  and  $C_0 = 1/2\sigma_{\theta 0}^2$ , equation (8) can be simplified as

$$F = \frac{z_0 z_2}{z_0 + z_2} \left( 1 + \frac{\sigma_{\theta 0}^2 z_0^2 + \sigma_{x0}^2}{2\sigma_{\theta 0}^2 z_0 z_2} \left\{ 1 - \left[ 1 - \frac{4\sigma_{x0}^2 \sigma_{\theta 0}^2 z_2^2}{(\sigma_{\theta 0}^2 z_0^2 + \sigma_{x0}^2)^2} \right]^{1/2} \right\} \right), \quad (10a)$$

$$\sigma_{x3} = F \sigma_{\theta 0} \sigma_{x0} / [\sigma_{x0}^2 + \sigma_{\theta 0}^2 (F - z_0)^2]^{1/2}, \quad (10b)$$

$$\sigma_{\theta 3} = [\sigma_{\theta 0}^2 (F - z_0)^2 + \sigma_{x0}^2]^{1/2} / F, \quad (10c)$$

$$z_2 = F [z_0 (z_0 - F) \sigma_{\theta 0}^2 + \sigma_{x0}^2] / [\sigma_{x0}^2 + \sigma_{\theta 0}^2 (z_0 - F)^2]. \quad (10d)$$

The focusing size  $\sigma_{x3}$ , divergence  $\sigma_{\theta 3}$  and focus distance  $z_2$  given in (10b), (10c) and (10d) are the same as equation (B14) in an early publication (Meron *et al.*, 1999) (except in that paper  $z_2 < 0$  when the focus point is downstream of the optics while by our definition it means  $z_2 > 0$ ). Directly using equation (10) to calculate  $F$  will cause ‘divided by zero’ errors at both  $z_0 = -z_2$  and  $z_0 = 0$  conditions; therefore  $F$  is derived further for these conditions as

$$F|_{z_0=-z_2} = z_2 (\sigma_{x0}^2 + \sigma_{\theta 0}^2 z_0^2) / (\sigma_{x0}^2 - \sigma_{\theta 0}^2 z_0^2), \quad (11a)$$

$$F|_{z_0=0} = \left[ 1 - \left( 1 - 4\sigma_{\theta 0}^2 z_2^2 / \sigma_{x0}^2 \right)^{1/2} \right] \sigma_{x0}^2 / 2\sigma_{\theta 0}^2 z_2. \quad (11b)$$

It is useful to further examine the above results under the following focusing situations:

(a)  $\sigma_{\theta 0} z_0 \gg \sigma_{x0}$ , *i.e.* the beam size at the optics,  $(\sigma_{\theta 0}^2 z_0^2 + \sigma_{x0}^2)^{1/2}$ , is much larger than the source size,  $\sigma_{x0}$ . Another assumption which we take for granted at synchrotron beamlines is that the focus distance  $z_2$  may not be much larger than the source distance  $z_0$  (actually  $z_2$  is typically smaller than  $z_0$ ). Equation (10) then becomes  $1/F = 1/z_0 + 1/z_2$  and  $\sigma_{x3} = \sigma_{x0} z_2 / z_0$ , the very familiar Gaussian lens equation for imaging used by beamline scientists for beamline designs.

(b)  $\sigma_{\theta 0} z_0 \ll \sigma_{x0}$  and  $\sigma_{\theta 0} z_2 \ll \sigma_{x0}$ , *i.e.* the beam size at the optics location is close to the source size and the focus distance is also short. This matches the secondary focusing situation when the secondary source is near the secondary optics. This is also the situation of the capillary secondary focusing performed at 18-ID with pre-focused beam right at the capillary entrance. Under these conditions, equation (10) becomes simply

$$F = z_2, \quad (12a)$$

$$\sigma_{x3} = z_2 \sigma_{\theta 0}, \quad (12b)$$

$$\sigma_{\theta 3} = \sigma_{x0} / z_2, \quad (12c)$$

which tells us that there will be focusing under this condition. This is different from the ‘common sense’ conclusion based on the geometrical optics image equations (*i.e.*  $1/F = 1/z_0 + 1/z_2$  and  $\sigma_{x3} = \sigma_{x0} z_2 / z_0$ ), which suggests no imaging when  $z_0 \rightarrow 0$ .

On the other hand, the beam size at the optics can also be close to the source size when the incident beam is highly collimated. In that case, equation (12) mostly matches our common-sense intuition.

### 2.3. Some characteristics of focusing

**2.3.1. Two different types of focusing measurement.** The beam size given by equation (7) is a function of both optical focal length  $F$  and focus distance  $z_2$ , therefore it has different minimal values along different paths of its two-dimensional variable space, at either  $\partial \sigma_{x3} / \partial z_2 = 0$  or  $\partial \sigma_{x3} / \partial F = 0$ . We used  $\partial \sigma_{x3} / \partial z_2 = 0$  as the focusing definition in this paper because of its unique property of decoupled intensity distribution in phase space. When we search along the beam path for a minimal spot after a beamline is focused, we are looking for the  $\partial \sigma_{x3} / \partial z_2 = 0$  focusing. However, if we tune the optics to achieve a minimal spot at a given sample location, we find the minimum of  $\partial \sigma_{x3} / \partial F = 0$ . Just for the convenience of discussion in this paper, we call the two minimums at  $\partial \sigma_{x3} / \partial z_2 = 0$  and  $\partial \sigma_{x3} / \partial F = 0$  the focus along distance  $z_2$  and focus along focal length  $F$ , respectively (but keep in mind the focus along the focal length is not a real focus in a certain perspective; for example, the beam intensity at the ‘focus along the focal length’ is still coupled among its two conjugated coordinates). With  $z_2$  at the position of focus along  $F$ ,  $\partial \sigma_{x3} / \partial F = 0$  makes

$$F = \Delta z_2 / (\Delta + \varphi z_2), \quad (13a)$$

$$\sigma_{x3} = z_2 (M / 2\Delta)^{1/2}, \quad (13b)$$

$$\sigma_{\theta 3} = (M / 2\Delta + \Delta / 2Q_0 z_2^2)^{1/2}, \quad (13c)$$

and at a given location  $z_2$  the  $\sigma_{x3}$  calculated using (13b) is smaller than the spot size calculated by (8b). With an incident beam described by its source parameters (*i.e.*  $B_0 = 0$ ) and a optical element having no slope errors ( $\alpha_s = 0$ ), equation (13) becomes

$$F = z_2 (z_0^2 \sigma_{\theta 0}^2 + \sigma_{x0}^2) / (z_0^2 \sigma_{\theta 0}^2 + \sigma_{x0}^2 + z_0 z_2 \sigma_{\theta 0}^2), \quad (14a)$$

$$\sigma_{x3} = z_2 \sigma_{\theta 0} / (1 + z_0^2 \sigma_{\theta 0}^2 / \sigma_{x0}^2)^{1/2}. \quad (14b)$$

**Table 1**

18-ID optical element major parameters (not all used at the same time; see text).

All units are meters.

Optics	Sagittal crystal	Vertical mirror	Capillary	KB mirror (V)	KB mirror (H)
Distance from source	54	56	70	70	70.2
Dimension along beam path		0.6	0.04	0.20	0.20
Focus distance			0.024†	0.42	0.22

† Capillary focus distance measured from the tip of the capillary, not from its center.

Both focusing along  $F$  and focusing along  $z_2$  are equivalent to the familiar equations of imaging by a lens ( $1/F = 1/z_0 + 1/z_2$  and  $\sigma_{x3} = \sigma_{x0} z_2 / z_0$ ) when  $\sigma_{\theta 0} z_0 \gg \sigma_{x0}$ ; when  $\sigma_{\theta 0} z_0 \ll \sigma_{x0}$  and  $\sigma_{\theta 0} z_2 \ll \sigma_{x0}$ , both can be approximated by equation (12), but are slightly different in higher-order terms. Taking the 18-ID horizontal KB mirror secondary focusing arrangement as an example (focus distance of 220 mm), assuming varying source distance relative to the secondary source (at 70 m from undulator source) generated by the beamline sagittal focusing (more information is given in §4 and Table 1), and treating the mirror as a thin lens, the required focal length and the focused beam size of the secondary focusing under both conditions of focusing along  $F$  and focusing along  $z_2$  are show in Fig. 3. The maximum differences between the two focusing modes occur around  $z_0 = 0$  (*i.e.* source on optics), and it can be derived from (11) and (14) for  $z_0 = 0$  that

$$(F_f - F_z) / F_f = \sigma_{\theta 0}^2 z_2^2 / \sigma_{x0}^2, \quad (15a)$$

$$(\sigma_f - \sigma_z) / \sigma_f = \sigma_{\theta 0}^2 z_2^2 / 2\sigma_{x0}^2, \quad (15b)$$

where the subscripts  $f$  and  $z$  are for focusing along  $F$  and focusing along  $z_2$ , respectively, and the  $(\sigma_{\theta 0} z_2 / \sigma_{x0})^2 \ll 1$

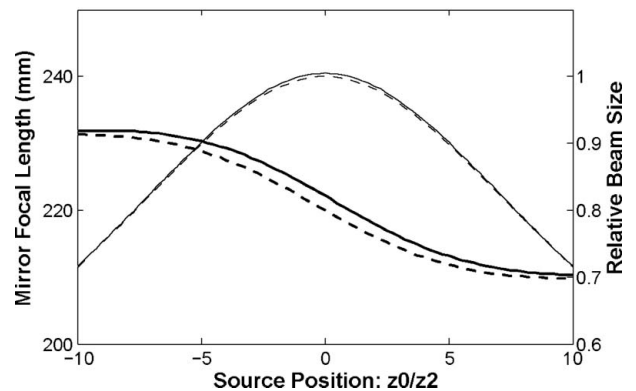


**Figure 3**

Around  $z_0 = 0$ , the differences between the focus along distance (solid lines) and focusing along focal length (dashed lines) reach maximums, which are still quite small for the focusing at 18-ID by the horizontal KB mirror, with 9% difference of focal length (thick lines) and 5% difference of focusing size (fine lines). The optics demagnification depends more on source size and divergence than the ratio of source to focus distances as  $|z_0/z_2|$  becomes small. Focal length changes smoothly when  $z_0 \rightarrow 0$  and  $z_0 \rightarrow -z_2$ . The relative beam size is the focusing size divided by  $\sigma_{\theta 0} z_2$ , the maximal focusing size with the source on the optics.

approximation is used, which is always valid for a demagnification situation, because  $\sigma_{\theta 0 z_2} / \sigma_{x_0}$  is the magnification factor when  $z_0 = 0$ . For the 18-ID horizontal KB mirror, the maximal relative differences between the two kinds of focusing are only 0.9% and 0.5%, respectively, for their focal lengths and focused spot sizes (Fig. 3). So, normally, we should not see the difference between the two kinds of focusing measurement in X-ray beamlines.

**2.3.2. Beam demagnification factor and optical focal length.** When the beam size at the optics location is much larger than the source size,  $1/F = 1/z_0 + 1/z_2$  and  $\sigma_{x_3} = \sigma_{x_0} z_2 / z_0$  can be used. When the beam size at the optics is not much larger than the source size (for example, when the source is close to the optics), the situation can be visualized as in Fig. 3. With a given focus distance, when  $|z_0/z_2|$  becomes smaller, the beam demagnification factor becomes less relevant to the ratio of source-to-focus distances. As for the optical focal length, it changes smoothly (and remains continuous) when  $z_0 \rightarrow 0$  or  $-z_2$ . In short, they are related not only to the ratio of source-to-focus distances but also to the incident beam size and divergence.

**2.3.3. Aperture effect on focusing.** It is well known that, when imaging an object with a lens under paraxial condition, the lens equation does not depend on the aperture size at the lens location. For the focusing of an X-ray beam with its parameters described at the optics location (*i.e.*  $z_0 = 0$  but  $B_0 \neq 0$ ) by  $\exp(-A_0 x_0^2 - 2B_0 x_0 \theta_0 - C_0 \theta_0^2)$ , equation (13) becomes

$$F = C_0 z_2 / (C_0 - B_0 z_2), \quad (16a)$$

$$\sigma_{x_3} = z_2 / (M/2C_0)^{1/2}, \quad (16b)$$

where the optical focal length  $F$  and focusing size  $\sigma_{x_3}$  are no longer dependent on  $A_0$ . If there is an aperture at the optics location described by a transmission function  $\exp(-Ax_0^2)$  (Pedersen & Riekkel, 1991; Meron *et al.*, 1999; Smilgies, 2008; Ferrero *et al.*, 2008) where  $A$  is a coefficient related to aperture opening, only  $A_0$  of the beam parameters will change after slitting. Since  $A_0$  is not in the calculation of focusing in equation (16), the aperture does not affect the focusing. Since the two types of focusing measurement are almost the same at demagnification beamlines, we conclude that, for both kinds of focusing, to focus part of a beam requires the same  $F$  to focus the whole beam.

## 2.4. More about focusing, imaging and phase-space analysis

Since the distribution of a beam is always decoupled among its two conjugated coordinates at a focus position (the focus along distance), if the optics are perfect without any errors the beam source parameters ( $\sigma_{x_0}, \sigma_{\theta 0}, z_0$ ) and focused parameters ( $\sigma_{x_3}, \sigma_{\theta 3}, z_2$ ) are exchangeable in equation (10). On the other hand, at an image location determined by the lens equation, the beam intensity distribution in phase space, generally speaking, is coupled.

It is also worthwhile mentioning that, as with the lens equation, the method for trapezoidal mirror analysis using an ellipse (or using a hyperbola for a virtual source) as reference

is not accurate when the condition  $\sigma_{\theta 0} z_0 \gg \sigma_{x_0}$  is not satisfied, even when the paraxial approximation may still be valid.

It can also be noted from equation (8) that the focusing of a beam is always possible as long as

$$z_2 \leq (\sigma_{\theta 0}^2 z_0^2 + \sigma_{x_0}^2) / 2[\sigma_{x_0}^2 \sigma_{\theta 0}^2 + \alpha_s^2 (\sigma_{x_0}^2 + \sigma_{\theta 0}^2 z_0^2)]^{1/2} \quad (17)$$

is satisfied. This limit of  $z_2$ , which has no significance for a non-extended source with negligible slope errors in the optics [when  $\sigma_{x_0} = 0$  and  $\alpha_s = 0$ , equation (17) becomes  $z_2 \leq \infty$ ], is required to keep the optic focal length real in equation (8a) or equation (10a).

## 3. Secondary micro-focusing analysis

### 3.1. Secondary focusing with capillaries for maximal flux

Detailed results of secondary focusing with a capillary at 18-ID have been reported recently (Barrea *et al.*, 2009). The primary focusing at 18-ID was achieved horizontally by a sagittal Si(111) crystal and vertically by a bimorph mirror, with their locations and major parameters given in Table 1. The focusing spot of the primary optics at 70 m from the source was about 120  $\mu\text{m}$  FWHM (V) by 220  $\mu\text{m}$  FWHM (H). A 40 mm-long single-bounce capillary with a focus distance of 24 mm (measured from its tip) was positioned exactly at the beamline secondary source position in order to maximize its acceptance. It delivered a secondarily focused round spot of less than 10  $\mu\text{m}$  FWHM with a total flux of  $3.3 \times 10^{12}$  photons  $\text{s}^{-1}$  (Barrea *et al.*, 2009). The capillary was of the single-bounce type that geometrically coincides with a small section of an ellipsoid with its two foci located at the X-ray source and sample locations (Balaic *et al.*, 1995; Bilderback & Huang, 2001). Since the synchrotron source–capillary distance is much larger than the capillary–sample distance, the average ‘focal length  $F$ ’ of the capillary is approximately the average distance the X-rays travel from the capillary to the sample, which is about 40 mm for this capillary. Given the APS undulator A nominal r.m.s. parameters ( $\sigma_x = 271.2 \mu\text{m}$ ,  $\sigma_{x'} = 11.4 \mu\text{rad}$ ,  $\sigma_y = 8.6 \mu\text{m}$ ,  $\sigma_{y'} = 2.9 \mu\text{rad}$ ) and undulator length  $L = 2.4$  m, the horizontal FWHM beam size at the sagittal crystal is about 1500  $\mu\text{m}$ , and the vertical FWHM size at the vertical mirror location is about 800  $\mu\text{m}$ , at 10 keV, which gives a focused beam divergence, before entering the capillary, of 90  $\mu\text{rad}$  (H) and 60  $\mu\text{rad}$  (V). With  $F = 40$  mm, equation (12) predicts a focusing size of 2.4  $\mu\text{m}$  (V)  $\times$  3.6 (H)  $\mu\text{m}$  FWHM, right at the capillary focusing position [from equation (12a),  $Z_2 = F$ ]. With the known angular averaging effect by capillary focusing (Huang & Bilderback, 2001, 2006), that prediction just matches the previously reported ray-tracing results of 3  $\mu\text{m}$  if the capillary had negligible figure errors (Barrea *et al.*, 2009). The measured  $\leq 10 \mu\text{m}$  focusing size can be explained by including capillary slope errors in the simulation.

### 3.2. Secondary micro-focusing with trapezoidal KB mirrors

**3.2.1. Calculation of secondary focusing with focusing formulas.** The trapezoidal micro-focusing KB mirrors used at 18-ID were designed with the taper factors of the substrates

optimized for directly focusing the synchrotron source without using any pre-focusing. In this section we evaluate the possibility of pre-focusing the X-rays by calculating the mirror shape required to focus the secondary virtual source, and then we check whether the mirror can be bent to match that shape with negligible or very small residual figure errors. We perform the analysis in two iterations. First, we take the beam parameters at the synchrotron X-ray source ( $B_0 = 0$ ) as the source used in equation (6) to calculate the beam parameters at the KB mirror location ( $A_3, B_3, C_3$ ). For simplicity, the primary focusing optics is treated as a thin lens with negligible dimensions along the beam path, therefore  $z_0$  and  $z_2$  are constant for all X-rays. Then, we use the above calculated result at the KB mirror location as the incident beam parameters in equation (8) to calculate the KB mirror focal length  $F$  for secondary focusing, and the  $z_0 = 0$  condition is used (but  $B_0 \neq 0$ , because the beam spatial and angular profiles are coupled at the KB mirror location). Because the micro-focusing mirror length is comparable with the focus distance,  $z_2$  will be a function of the reflecting position  $z$  along the mirror length, and the calculated focal length  $F$  will also be a function of  $z$ . The mirror slope  $S(z)$  and curvature  $R(z)$  can be calculated from  $F(z)$ , with

$$S'(z) = (1 + S^2)^{3/2} \sin(\theta + S) / 2F(z), \quad (18a)$$

$$R(z) = 2F(z) / \sin(\theta + S), \quad (18b)$$

where  $\theta$  is the X-ray incident angle to the mirror at the mirror center where both  $z$  and  $S$  are assumed to be zero, and  $S'$  is the first derivative of  $S$  with respect to  $z$ .

The above calculated  $F(z)$  is the focal length of a thin lens needed at position  $z$  to focus the whole beam. It is concluded in §2.3 that to focus part of a beam requires the same  $F$  as to focus a whole beam, therefore  $F(z)$  is also the focal length of every little part of a mirror with varying  $F$  when the mirror has an asymmetric bending to focus the whole beam.

The substrates of the 18-ID trapezoidal micro-focusing mirrors have uniform thickness but with a tapered width changing along the mirror length, and each mirror is operated with two independently adjustable bending moments on two ends (Yang *et al.*, 1995; Eng *et al.*, 1998). With the given source and sample distances and the given mirror reflecting angle, the mirror taper factor  $\alpha$  and mirror bending moment asymmetry factor  $\eta$  (for definitions, see Eng *et al.*, 1998) can be optimized, in general, by fitting the following bent-mirror slope profile,

$$S(z) = -\frac{k_0 f'}{\alpha^2} \left[ \eta \alpha \frac{z}{f'} + (\eta + \alpha) \ln \left( 1 - \alpha \frac{z}{f'} \right) \right], \quad (19)$$

to an ideal ellipse (Eng *et al.*, 1998). In (19),  $k_0$  is the inverse of the mirror central radius of curvature,  $f' = F/\cos(\theta)$  and  $F$  is the focal length at the mirror center. In the Bio-CAT situation, since the KB mirrors are already made with taper factors optimized for directly focusing the synchrotron source, we only need to optimize the mirror bending asymmetry factor  $\eta$  using least-squares fitting to minimize the difference between the profiles calculated from (18) and (19). That minimized difference is the mirror residual figure error.

When the beamline secondary source is on the secondary optics, the total flux to the final focus is maximized. That flux can decrease by either increasing the primary optics focal length (we can call it ‘pre-underfocusing’) or decreasing the primary optic focal length (we can call it ‘pre-overfocusing’). Figs. 4 and 5 show the calculated results for the horizontal secondary focusing of the 18-ID KB mirror for pre-underfocused beams, covering the situation from no pre-focusing to having pre-focused beam right at the KB mirror. The secondary sources within this range are mainly virtual with respect to the KB mirrors. In our calculations the mirror optical length is chosen as 150 mm to match the 600  $\mu\text{m}$  slit opening used in front of the mirrors; the incident angle  $\theta$  is 4.0 mrad; the sample to horizontal KB mirror center distance is 220 mm; and the assumed mirror slope errors are 1.7  $\mu\text{rad}$ . The horizontal mirror substrate is 200 mm long with upstream and downstream widths of 46 mm and 13.2 mm, respectively.

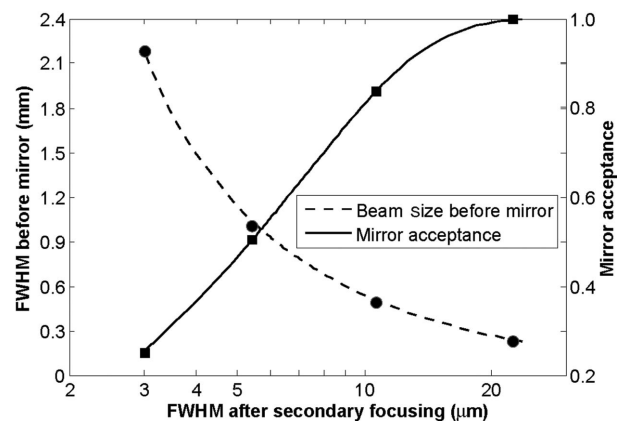


**Figure 4** The solid and dashed lines are the calculated mirror acceptance and pre-focused beam size at the KB mirror location *versus* secondary focusing size, for horizontal KB mirror focusing of ‘pre-underfocused’ sources at 18-ID. As a comparison, *SHADOW* ray-tracing simulations of secondary focusing are also performed for four different pre-focusing conditions, using the KB mirror shapes calculated based on the phase-space analysis. For simplicity, the secondary focusing sizes are calculated with the focus distance measured from the mirror center.

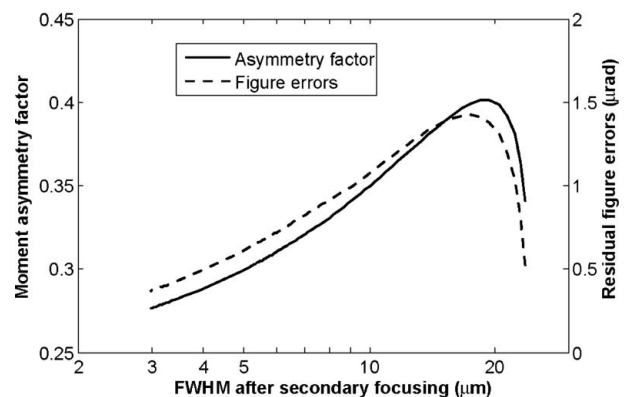


**Figure 5** The simulated horizontal mirror bending asymmetry factor (solid line) and the residual figure errors (dashed line) *versus* secondary focusing size, for the 18-ID horizontal KB mirror focusing of ‘pre-underfocused’ virtual sources.

The APS nominal source emittance (given in §3.1) is used and the undulator source size is calculated at an X-ray energy of 12 keV. Slope errors of 1.8  $\mu\text{rad}$  are applied to the sagittal crystal so that the minimum achievable focusing spot of the primary horizontal focusing at the KB mirror location matches the measured 220  $\mu\text{m}$  (FWHM). According to the results shown in Figs. 4 and 5, it is possible to increase the acceptance of the KB mirrors with only a moderate sacrifice of the final focusing spot size. While the incident beam size at the KB mirror location is focused from 2.2 mm down to 0.6 mm, the total flux increases by a factor of three and the beam size also increases by a factor of three. According to Fig. 4, with a final focusing size of about 15  $\mu\text{m}$ , the horizontal mirror acceptance becomes close to 100%. When the mirror acceptance reaches 90%, further focusing of its incident beam only increases the secondary focusing size but with little increase of flux, since the incident beam size is already much smaller than the mirror acceptance. The mirror bending moment asymmetry factor only changes moderately (Fig. 5), and the simulated mirror central focal length, an indication of the average bending, only changes by about 6% (not shown in the figures); all these can be satisfied easily by adjusting the two bending forces at the mirror's two ends. The residual mirror figure errors only increase gradually with the increase of pre-focusing and are only about 1  $\mu\text{rad}$  when the incident beam is almost fully focused on the KB mirrors (the maximized acceptance condition); therefore they have a negligible effect on the secondary focusing quality (Fig. 5).

**3.2.2. Verifying the calculation of secondary focusing by ray-tracing.** In the above analysis, we have already calculated the mirror bending shape for given pre-focused conditions; therefore it was straightforward for us to use *SHADOW* ray-tracing (Welnak *et al.*, 1994), an extension tool included in the *XOP* software package (Sanchez del Rio & Dejus, 2004), to verify the analytically calculated KB secondary focusing. For ray-tracing of pre-focusing, we used different 'spherical radius' values for the sagittal bent crystal to create the different pre-focused spot sizes at the KB mirror location. The slope errors of the sagittal crystal were simulated as its 'modified surface error'. For secondary focusing, the KB mirror bending was simulated as the modified surface error of a plane mirror, with the profile calculated from the integration of equation (19),

$$y(z) = -\frac{\eta k_0 z^2}{2\alpha} + \frac{(\eta + \alpha)k_0 f'^2}{\alpha^3} \left\{ \left(1 - \alpha \frac{z}{f'}\right) \times \left[ \ln\left(1 - \alpha \frac{z}{f'}\right) - 1 \right] + 1 \right\}, \quad (20)$$

where  $y(z)$  is the mirror surface height relative to a flat mirror. Finally, the ray-traced spot size was corrected with a beam size broadening of 1.76  $\mu\text{m}$  by the assumed 1.7  $\mu\text{rad}$  (r.m.s.) KB mirror slope errors. With the above steps, we ray-traced the secondary focusing for four different pre-focused beam sizes at the KB mirror location: 225  $\mu\text{m}$  (fully focused), 0.5 mm, 1.0 mm and 2.15 mm (unfocused), and the results match our phase-space calculation very well, as shown in Fig. 4.

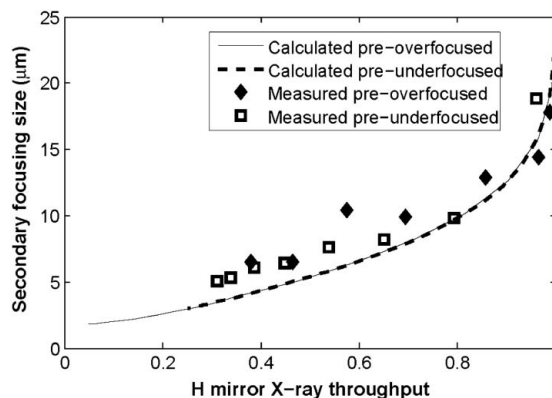


**Figure 6**

The calculated and measured horizontal focusing sizes *versus* horizontal mirror throughput for the 18-ID KB mirror, concluding that a micro-focusing trapezoidal mirror can be bent accordingly to trade beam size with acceptance; final focusing size is not affected by whether the incident beam is pre-overfocused or pre-underfocused. While pre-overfocusing may have the potential of making smaller beam size with sacrificing acceptance, it is not pursued at 18-ID. Mirror throughput is normalized to the maximum flux, when a fully pre-focused beam, about 220  $\mu\text{m}$ , is on the mirror.

**3.2.3. Pre-overfocusing versus pre-underfocusing.** We also carried out a similar analysis for the case of pre-overfocused beam secondary focusing, and we found out that, as for the relationship between the KB mirror acceptance and secondary focusing spot size, both 'pre-overfocusing' (real secondary source) and 'pre-underfocusing' (virtual secondary source) yield similar results (Fig. 6), though the bending of the KB mirrors will be different for each case. This is in agreement with Liouville's theorem: at the mirror focus, the product of beam divergence and beam focal size is approximately the phase-space area of the beam accepted by the mirror, with beam divergence almost the same for different pre-focusing conditions because it is mostly determined by mirror size and focus distance; less KB mirror acceptance of the secondary source, whether it is pre-overfocusing or pre-underfocusing, means less X-ray phase-space area that the mirror is accepting, therefore the smaller focusing size the KB mirror can make given that the beam divergence after the KB mirror is almost the same. The same analysis has also been carried out for the vertical KB mirror with similar results but with much smaller mirror bending residual errors, which is to be expected owing to its larger focus distance (420 mm).

#### 4. Test of secondary micro-focusing using KB mirrors at 18-ID

The Bio-CAT microprobe (Barrea *et al.*, 2006) is dedicated to X-ray fluorescence microscopy and X-ray absorption micro-spectroscopy experiments on biological tissue sections, with optics comprising a KB mirror bender system of the University of Chicago design (Eng *et al.*, 1998) with two Rh-coated silicon mirrors (see Table 1). The bender system relies on high-precision Newport stages to provide the four required degrees of freedom per mirror: translation, tilt/rotation and upstream

and downstream bending. In its standard operation configuration the KB mirror system delivers a  $\leq 5 \mu\text{m}$  FWHM (V and H) size beam and  $1.3 \times 10^{12}$  photons  $\text{s}^{-1}$  flux at 12 keV without pre-focusing. There are special cases where the microbeam size requirements might be relaxed somewhat in favour of higher delivered flux. For instance, when  $10 \mu\text{m}$ -thick tissue sections are analyzed for their metal content, it is extremely important to maximize the flux delivered on the sample in order to generate sufficient characteristic fluorescence photons in order to be detected.

We have tested the optical configuration suggested by the above calculations that would provide a significant increase in photon flux by pre-focusing the monochromatic beam using the beamline main optics. The micro-focusing KB mirrors used at 18-ID, with an acceptance of about  $600 \mu\text{m}$  in both transverse directions, accept a large fraction of the beam in the vertical direction but only a small fraction in the horizontal direction. The beamline primary horizontal focusing with a sagittal crystal can be easily implemented without affecting the downstream beam position, while the primary vertical focusing with a mirror will change the downstream beam direction and equipment offset. So, in this test, we were only interested in pre-focusing the beam horizontally. A set of slits with opening of  $600 \mu\text{m} \times 600 \mu\text{m}$  located just upstream of the KB mirrors work as beam defining slits, limiting the incident beam to the acceptance of the mirrors. Two ion chambers mounted just upstream and downstream of the mirrors monitored the incident and delivered beam intensity. A  $\text{CdWO}_4$  (cadmium tungstate) fluorescence crystal set at the sample location together with a Hitachi camera with infinity optics were used to visualize the secondarily focused beam. The KB mirror focusing adjustment is judged visually through a video camera, followed by a measurement of the X-ray fluorescence emission of a Ni thin film supported by a Si wafer (knife-edge scan) in order to determine the beam size.

We measured the secondarily focused beam horizontal size at 12 keV under varying sagittal focusing, from pre-under-focused to pre-over-focused condition. The horizontal mirror throughput was calculated using the ion chamber readings. The results in Fig. 6 are showing the flux increase of more than a factor of three just by the horizontal pre-focusing alone, with the beam size increasing from  $\sim 5 \mu\text{m}$  to  $\sim 18 \mu\text{m}$ . It can also be seen from both the analytical results and test results in Fig. 6 that the secondarily focused size has the same relationship with mirror acceptance under both primary underfocusing and overfocusing situations, although at 18-ID we are more interested in the pre-underfocusing conditions because it is easier to implement. It is also shown in Fig. 6 by calculation that the pre-overfocusing could possibly decrease the secondary focusing size compared with the non-prefocused condition, but with a sacrifice of flux. This is beyond our current test scope and interest at Bio-CAT.

Some of the discrepancy between the experiment data and calculated results in Fig. 6 may result from the following factors: uncertainty while visually judging the focusing of a few micrometers spot *via* a video camera; possible slight focusing, by the sagittal crystal, at the presumed non-focusing condition,

affecting the accuracy of data near non-pre-focused conditions.

## 5. Conclusions and discussion

### 5.1. Conclusions

Focusing an X-ray beam could be quite different than imaging its source, especially with secondary focusing at an X-ray beamline because the secondary source could be very close to, or on, the optics. Some details of the focusing of a beam with Gaussian profile by a thin lens were elucidated in phase space, which is applied to secondary focusing calculations: when the criterion  $\sigma_{\theta_0 z_0} \gg \sigma_{x_0}$  [*i.e.* the beam size at optics,  $(\sigma_{\theta_0 z_0}^2 + \sigma_{x_0}^2)^{1/2}$ , is much larger than the source size,  $\sigma_{x_0}$ ] is not satisfied, the normal methods we use for beamline optics design, such as the thin-lens equation, the comparison of mirror shape to an ellipse or hyperbola, will not be valid; new focusing formulas have been developed for general conditions of source under the paraxial approximation; slope errors are successfully included in these formulas so that they can be used to calculate beamline focusing with good accuracy. At the focus, the beam intensity distribution is decoupled among its conjugated coordinates in phase space, even after an optical element with slope errors; focus along focal length (not exactly the focus because the intensity profile is still coupled) and focus along distance (the real focus by definition) are both equivalent to the image by a lens when  $\sigma_{\theta_0 z_0} \gg \sigma_{x_0}$ ; for the optics having a demagnification while  $z_0 \simeq 0$  (*i.e.*  $\sigma_{\theta_0 z_0} / \sigma_{x_0} \ll 1$ ), both ways of focusing are approximately the same with a source at any location; slits approximated by Gaussian transmission functions at the location of the optics do not change the focusing properties. A method of using thin-lens focusing formulas given in this paper to evaluate the focusing by an asymmetrically bent mirror has been introduced.

The 18-ID horizontal KB mirror secondary focusing is analysed based on the above thin-lens formulas. Both analytical and experimental results concluded that it is possible to use trapezoidal mirrors to focus the incident X-rays that have been pre-focused to various locations along the beam path, leading to different flux acceptances by the KB mirrors. Secondary focal spot size depends on the pre-focused spot size measured at the position of the KB mirrors. The vertical KB mirror can also secondarily focus a pre-focused beam according to this analysis. However, at 18-ID, the vertical KB mirror acceptance is already sufficiently large without pre-focusing given the smaller vertical beam size, thus we did not pursue it experimentally. The capillary secondary focusing done previously at 18-ID is also explained by this analysis.

### 5.2. Discussions about secondary focusing

There is also a 'favourable' pre-focusing range beyond which further pre-focusing may not be worthwhile. At 18-ID, for example, when the KB mirror acceptance is around 80–90%, a further decrease in the pre-focused beam size at the KB mirror location will further increase the final focusing size with little increase in flux (see the curves in Fig. 6, or Fig. 4).

Therefore, there seems to be an optimal size of a KB mirror (and therefore its focus distance), and with this optimized mirror size the mirror will just accept about 80–90% of a fully pre-focused beam. In that case the whole beamline optical system will have a larger adjustable range of final focal spot size and X-ray acceptance.

In this paper we discussed secondary focusing with examples of micro-focusing mirrors and a single-bounce capillary, though this analysis can be applied to other types of focusing optics. From equation (12) it can be seen that an optical device with a shorter focal length is always advantageous for generating smaller focusing size when the secondary source is on the optics for maximized flux. Capillaries could have an advantage over similar acceptance KB mirrors due to being more compact, with equal focal lengths in both transverse directions; however, the figure accuracy of current single-bounce capillaries still needs improvement before we can realise the full benefit from using a capillary with third-generation sources (though the quality is almost there). On the other hand, trapezoidal micro-focusing mirrors have the advantage of adjustable focal length to match incident beams with different degrees of pre-focusing.

Many thanks to Professor Thomas C. Irving for his careful reading and critical suggestions about the manuscript. Use of the Advanced Photon Source was supported by the US Department of Energy, Basic Energy Science, Office of Energy Research, under Contract No. W-31-109-Eng-38. IMCA-CAT is supported by the companies of the Industrial Macromolecular Crystallography Association. Bio-CAT is a NIH-supported Research Center, RR08630. ChemMatCARS is principally supported by the National Science Foundation/Department of Energy under grant number NSF/CHE-0822838. The content is solely the responsibility of the authors and does not necessarily reflect the official views of the National Center for Research Resources or the National Institutes of Health. Project also supported by award number R21CA139386 from the National Cancer Institute.

## References

- Balaic, D. X., Nugent, K. A., Barnea, Z., Garrett, R. & Wilkins, S. W. (1995). *J. Synchrotron Rad.* **2**, 296–299.
- Barrea, R. A., Gore, D., Kondrashkina, E., Weng, T., Heurich, R., Vukonich, M., Orgel, J., Davidson, M., Collingwood, J. F., Mikhaylova, A. & Irving, T. C. (2006). *Proceedings of the 8th International Conference on X-ray Microscopy, IPAP Conference Series 7*, pp. 230–232.
- Barrea, R. A., Huang, R., Cornaby, S., Bilderback, D. H. & Irving, T. C. (2009). *J. Synchrotron Rad.* **16**, 76–82.
- Bilderback, D. H. & Huang, R. (2001). *Nucl. Instrum. Methods Phys. Res. A*, **467–468**, 970–973.
- Eng, P. J., Newville, M., Rivers, M. L. & Sutton, S. R. (1998). *Proc. SPIE*, **3449**, 145–156.
- Ferrero, C., Smilgies, D.-M., Riekel, C., Gatta, G. & Daly, P. (2008). *Appl. Opt.* **47**, E116–E124.
- Gerrard, A. & Burch, J. M. (1975). *Introduction to Matrix Methods in Optics*. New York: John Wiley and Sons.
- Hastings, J. B. (1977). *J. Appl. Phys.* **48**, 1576–1584.
- Huang, R. & Bilderback, D. (2001). *Nucl. Instrum. Methods Phys. Res. A*, **467–468**, 978–981.
- Huang, R. & Bilderback, D. (2003). *AIP Conf. Proc.* **705**, 712–715.
- Huang, R. & Bilderback, D. H. (2006). *J. Synchrotron Rad.* **13**, 74–84.
- Matsushita, T. & Kaminaga, U. (1980a). *J. Appl. Cryst.* **13**, 465–471.
- Matsushita, T. & Kaminaga, U. (1980b). *J. Appl. Cryst.* **13**, 472–478.
- Meron, M., Viccaro, P. J. & Lin, B. (1999). *Phys. Rev. E*, **59**, 7152–7165.
- Mosselmanns, J. F. W., Quinn, P. D., Dent, A. J., Cavill, S. A., Moreno, S. D., Peach, A., Leicester, P. J., Keylock, S. J., Gregory, S. R., Atkinson, K. D. & Rosell, J. R. (2009). *J. Synchrotron Rad.* **16**, 818–824.
- Pedersen, J. S. & Riekel, C. (1991). *J. Appl. Cryst.* **24**, 893–909.
- Sanchez del Rio, M. & Dejus, R. J. (2004). *Proc. SPIE*, **5536**, 171–174.
- Smilgies, D.-M. (2008). *Appl. Opt.* **47**, E106–E115.
- Snigirev, A., Bjeoumikhov, A., Erko, A., Snigireva, I., Grigoriev, M., Yunkin, V., Erko, M. & Bjeoumikhova, S. (2007). *J. Synchrotron Rad.* **14**, 326–330.
- Welnak, C., Chen, G. J. & Cerrina, F. (1994). *Nucl. Instrum. Methods Phys. Res. A*, **347**, 344–347.
- Yang, B. X., Rivers, M., Schildkamp, W. & Eng, P. J. (1995). *Rev. Sci. Instrum.* **66**, 2278–2280.